


Review

Single-Molecule Surface-Enhanced Raman Spectroscopy

Yuxuan Qiu¹, Cuifang Kuang^{1,2,3}, Xu Liu^{1,2,3} and Longhua Tang^{1,*} 

¹ State Key Laboratory of Modern Optical Instrumentation, College of Optical Science & Engineering, Zhejiang University, Hangzhou 310027, China; yuxuanqiu@zju.edu.cn (Y.Q.); cfkuang@zju.edu.cn (C.K.); liuxu@zju.edu.cn (X.L.)

² Ningbo Research Institute, Zhejiang University, Ningbo 315100, China

³ Collaborative Innovation Center of Extreme Optics, Shanxi University, Taiyuan 030006, China

* Correspondence: lhtang@zju.edu.cn; Tel.: +86-571-87953066

Abstract: Single-molecule surface-enhanced Raman spectroscopy (SM-SERS) has the potential to detect single molecules in a non-invasive, label-free manner with high-throughput. SM-SERS can detect chemical information of single molecules without statistical averaging and has wide application in chemical analysis, nanoelectronics, biochemical sensing, etc. Recently, a series of unprecedented advances have been realized in science and application by SM-SERS, which has attracted the interest of various fields. In this review, we first elucidate the key concepts of SM-SERS, including enhancement factor (EF), spectral fluctuation, and experimental evidence of single-molecule events. Next, we systematically discuss advanced implementations of SM-SERS, including substrates with ultra-high EF and reproducibility, strategies to improve the probability of molecules being localized in hotspots, and nonmetallic and hybrid substrates. Then, several examples for the application of SM-SERS are proposed, including catalysis, nanoelectronics, and sensing. Finally, we summarize the challenges and future of SM-SERS. We hope this literature review will inspire the interest of researchers in more fields.

Keywords: surface-enhanced Raman spectroscopy; single-molecule detection; surface plasmon resonance; nanoparticle



Citation: Qiu, Y.; Kuang, C.; Liu, X.; Tang, L. Single-Molecule Surface-Enhanced Raman Spectroscopy. *Sensors* **2022**, *22*, 4889. <https://doi.org/10.3390/s22134889>

Academic Editor: Anna Chiara De Luca

Received: 31 May 2022

Accepted: 24 June 2022

Published: 29 June 2022

Publisher's Note: MDPI stays neutral with regard to jurisdictional claims in published maps and institutional affiliations.



Copyright: © 2022 by the authors. Licensee MDPI, Basel, Switzerland. This article is an open access article distributed under the terms and conditions of the Creative Commons Attribution (CC BY) license (<https://creativecommons.org/licenses/by/4.0/>).

1. Introduction

Raman scattering arises from the interaction between photons and molecules [1]. The molecular transition energy can be obtained by measuring the wavelength of Raman scattered photons. Thus, the Raman spectrum is also known as the chemical fingerprint spectrum [2]. Raman spectroscopy has the advantage of being label-free and non-invasive, so it is widely used in material and life science. However, spontaneous Raman scattering is very weak, with only 1 in 10^7 photons involved, which limits the sensitivity of Raman spectroscopy.

Surface-enhanced Raman spectroscopy (SERS) significantly enhances the Raman signal beyond the sensitivity limit of Raman spectroscopy [3]. In general, surface-enhanced Raman scattering occurs on molecules adsorbed on the rough surface or nanostructure of noble metal substrates. It is generally accepted that SERS enhancement is the result of electromagnetic mechanisms (EM) and chemical mechanisms (CM) [4,5]. EM enhancement is the dominant contribution of SERS. Surface plasmon resonance (SPR), the collective oscillation of free electrons excited by photons, localizes the electromagnetic field on the surface of the substrate. The strong, localized electromagnetic field amplifies the Raman signal of molecules adsorbed on the substrate. CM, providing less enhancement than EM, is employed as a complementary approach. The Raman polarizability tensor of analyte molecules is modified by charge transfer between molecules and hot electrons.

Single-molecule SERS (SM-SERS), the Raman spectrum from a single molecule, is the ultimate goal of SERS in terms of sensitivity (Figure 1). SM-SERS is an unprecedentedly

high-throughput and ultra-sensitive method for chemical analysis. More importantly, subtle spectroscopic phenomena from single molecules are observed without a statistical average. In application, SM-SERS has been widely used in various fields, including chemical analysis, nanoelectronics, and biochemical sensing [6–9]. For example, in situ monitoring of catalytic reactions could be achieved by SM-SERS. Monitoring at the single-molecule level reveals the mechanism of the reaction, thus guiding the design of highly efficient catalysts.

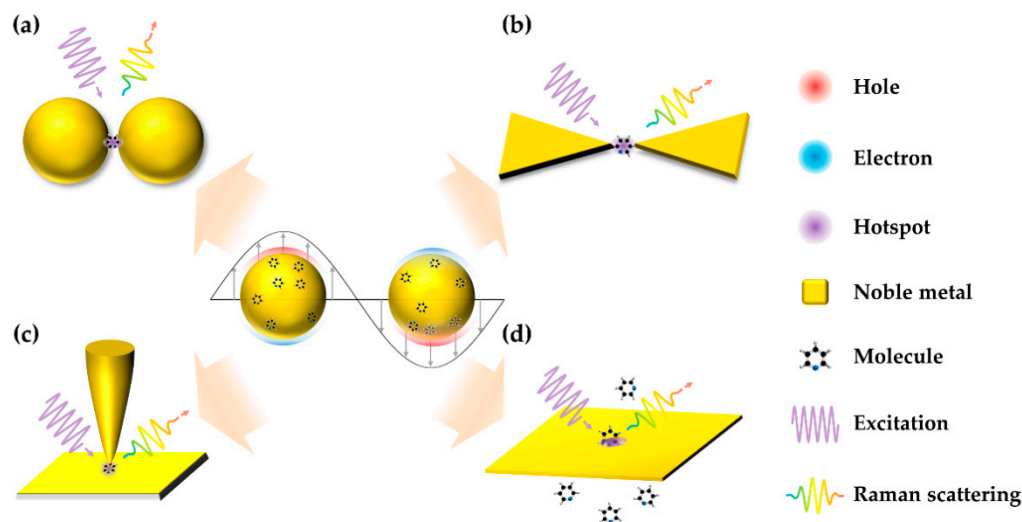


Figure 1. Schematic diagram of SM-SERS. Center: SPR effect of nanoparticles; Inset: (a) dimetric nanostructure; (b) plasmonic single-molecule junction; (c) plasmonic tip; (d) plasmonic nanopore.

It has been more than 20 years since SM-SERS was first reported in 1997 [10,11]. In these two decades, the theory of SM-SERS has undergone several changes, but some experimental phenomena have yet to be fully explained. A series of sophisticated schemes for SM-SERS has been proposed, with a strong localized electromagnetic field, high-reproducibility substrates, strategies for localizing molecules in hotspots, etc. Researchers are also extending SM-SERS to a variety of environments to accommodate more applications. In practice, some critical challenges still exist. In this review, we clarify the concepts of SM-SERS, evaluate the progress and challenges in SM-SERS, and illustrate applications of SM-SERS. We hope this literature review will inspire the interest of researchers in various fields.

2. Single-Molecule SERS

Measuring the structure and behavior of single molecules has attracted great attention in various fields. Several single-molecule detection techniques have been implemented [12,13], including transmission electron microscopy (TEM), scanning tunneling microscopy (STM), atomic force microscopy (AFM), tunneling sensing, single-molecule fluorescence microscopy, etc. SM-SERS detects the vibrational modes of single molecules, providing high-throughput structural information. SM-SERS could be flexibly applied in various environments, from ultra-high vacuum at cryogenic temperature to in a solution at room temperature [14,15]. In addition, SM-SERS plays an important role in catalysis, nanoelectronics, sensing, etc. SM-SERS has demonstrated exciting prospects in science and application. However, when the concentration of the analyte is decreased to a single-molecule level, extraordinary phenomena and problems appear. Several concepts of SM-SERS are worth clarifying.

2.1. Enhancement Factor

The enhancement factor (EF) of SERS is the ratio of Raman signal with and without substrates in the same measurement conditions, normalized for the number of molecules probed. The EF is defined as:

$$EF = \frac{I_{SERS}/N_{surf}}{I_{RS}/N_{vol}}, \quad (1)$$

where I_{RS} and I_{SERS} are the Raman intensity for N_{vol} molecules and SERS intensity for N_{surf} molecules.

EM-induced enhancement comes from two multiplicative effects: one results from enhancement of the local excitation field; the other is due to enhancement of the re-emitted Raman scattering [16].

$$G(r) = \left[\frac{E_{loc}(\omega_0, r)}{E_0(\omega_0, r)} \right]^2 \left[\frac{E_{loc}(\omega_R, r)}{E_0(\omega_R, r)} \right]^2, \quad (2)$$

where r is the spatial coordinate, ω_0 and ω_R are the frequency of excitation and Raman photons, $E_0(\omega, r)$ is the electric field of excitation light, and $E_{loc}(\omega, r)$ is the enhanced local electric field. Ignoring the frequency difference between the excitation and Raman photons, EM-induced enhancement is approximately proportional to the fourth power of the local electric field enhancement, which is known as the E^4 approximation [17].

CM-induced enhancement relies on modification of the Raman polarizability tensor of the analyte molecules by charge transfer. The overall SERS intensity $I(\omega_R)$ can be expressed as:

$$I(\omega_R) = AG(r)|\alpha(\omega_R, \omega_0)|^2 I_0(r, \omega_0) \quad (3)$$

where A is the collection efficiency of the setups, $\alpha(\omega_R, \omega_0)$ is the Raman polarizability of the molecule, and $I_0(r, \omega_0)$ is the intensity of excitation light.

The EF required to observe single-molecule events is critical but controversial. When SM-SERS was first observed, single-molecule events were observed when the molecules were adsorbed in the Ag colloid. It was claimed that an EF of 10^{14} is essential for single-molecule detection [11]. A series of subsequent studies revised the value to 10^7 – 10^8 [18,19].

Indeed, SERS intensity depends not only on the SERS substrates, it is also related to the analytes and optical setups. For analytes, various molecules differ in Raman scattering cross sections. In the same excitation conditions, the larger the differential cross sections, the more intense the Raman scattering [20]. Especially when the excitation wavelength corresponds to the electronic transition of a molecule, resonance enhancement of Raman scattering occurs. The excited electrons transition to the excited electronic state rather than a virtual state, significantly increasing the cross section, providing the EF of 10^2 – 10^6 [21]. As for optical setups [22], a high numerical aperture (NA) objective enables high Raman collection efficiency. The sensitivity of the spectrometer determines the lowest detectable intensity coupled to the spectrometer. In particular, when the wavelength and polarization of the excitation beam match the SPR of the SERS substrates, the highest EM-induced EF is obtained.

It is worth mentioning that the mechanism of some experimental phenomena of SM-SERS has not yet been fully explained. Several reports have proposed that some previously ignored physical mechanisms, such as Rayleigh scattering, discrete interaction, and quantum interaction need to be considered in SM-SERS [23–26].

2.2. Experimental Evidence of Single-Molecule Event

In earlier studies, the ultra-low concentration of the analyte was considered evidence for single-molecule detection, with less than one molecule in the probed volume on average [10]. However, due to the sparse distribution of hotspots, it is highly probable that no molecules are present in the hotspot in most events. Moreover, contamination, dilution errors, wall adsorption, and overestimation of hotspots affect the demonstration in such

a low concentration. Consequently, direct experimental evidence is required to prove the existence of a single-molecule event.

Fluctuations of SERS both in intensity and spectral shape were once considered the experimental evidence of single-molecule events [10,11]. In single-molecule level concentration, the dynamic movement of molecules in hotspots causes signal fluctuations. Nevertheless, later studies showed that the fluctuations are an intrinsic property of SERS rather than adequate evidence for SM-SERS [27]. Similar fluctuations were observed at higher concentrations [28]. More evidence was considered based on statistics. When the average number of molecules in the probed volume is one or less, the statistical distribution of the Raman signal changes from Gaussian to Poisson and is quantized to correspond to zero, one and two molecules in the probed volume [10,11]. It has been noted that inadequate sampling (e.g., 100) following a log-normal distribution often exhibits oscillations similar to a Poisson distribution [27]. More than 10^4 samplings are required for a rigorous argument [29].

Bianalyte's approach [30] provides direct experimental evidence for SM-SERS without relying on ultra-low concentration. In this approach, a mixture of two analytes with distinguishable Raman spectra are adopted for SERS measurement. With more than one molecule in the hotspot, the SERS is a mixture spectrum of both analytes. If only one molecule on average exists in the hotspot, the measured SERS signal comes from either one of the two analytes.

2.3. Spectral Fluctuation and Data Analysis

To retrieve chemical information from recorded Raman spectrum, many classification and dimensionality reduction algorithms are adopted to deal with SERS data, including support vector machine (SVM), principal component analysis (PCA), cluster analysis, and deep learning [31–33]. However, spectral fluctuations in SM-SERS inevitably disturbs data analysis, even though some digital signal processing methods are used to suppress the effects of fluctuation [27].

In contrast, spectral fluctuations and blinking imply single-molecule information. Lindquist et al. [34] proposed high-speed super-resolution imaging to capture the temporal and spatial features of fluctuation. The physical and chemical properties of molecules and substrates, including molecular adsorption and desorption, molecular reorientation, surface diffusion, and metal surface reconstruction [35,36], have been resolved through spectral fluctuation and blinking. Weber et al. [37] mapped the shape of hotspots from the fluctuation and studied the molecular motion of the nanoparticles. Furthermore, environmental factors such as temperature, pressure, light intensity, and charge transfer have been proven to influence spectral fluctuations [38–41]. So far, the principle of spectral fluctuation and blinking has not been fully understood. Therefore, the study of spectral fluctuation is not only conducive to the understanding of the single-molecule system, but also to the development of an analysis algorithm based on SM-SERS data.

3. Advanced Implementation of SM-SERS

According to the reports by Kneipp and Nie [10,11], SM-SERS measurements rely on the random adsorption of analyte molecules to the hotspots in colloidal silver solution. A series of surveys revealed that only the aggregation of multiple nanoparticles could provide enough EF for SM-SERS [28,42]. When the analyte molecule is localized at the gap between the nanoparticles, the Raman scattering is greatly amplified. Although single-molecule sensitivity has been realized in such a scheme, some drawbacks still exist. First, EF is highly sensitive to interparticle distance, which cannot be precisely controlled in colloidal silver. Second, the aggregation of nanoparticles is extremely heterogeneous, and few SM-SERS hotspots are generated, which makes analyte molecules in hotspots a rare event. Therefore, an advanced SM-SERS scheme has been developed around two aspects: SERS substrate with ultra-high EF and reproducibility, and improving the probability of analyte molecules in hotspots. On the other hand, conventional SERS substrate material is dominated by a

noble metal. The development of nonmetallic and hybrid substrates is beneficial to broaden the application of SM-SERS.

3.1. Substrates with Ultra-High EF and Reproducibility

Single nanoparticles typically do not provide enough EF for SM-SERS, and only the gaps between nanoparticles are active sites. The nanoscale error of gaps causes an EF difference up to several orders of magnitude. Nevertheless, such sites are sparse in colloidal silver. Less than 5% of sites contribute more than 80% of the overall SERS intensity [43]. Thus, constructing highly reproducible substrates is crucial for SM-SERS.

Dimer, as a simple and effective nanostructure, is widely adopted in SM-SERS due to its ultra-high EF in the nanogap. Lim et al. [44] reported a reproducible dimetric nanostructure, called gold–silver core–shell nanodumbbell (GSND) (Figure 2a). GSND consists of two Au nanoparticles with an Ag shell linked by DNA strands. A dye molecule attached to the DNA strand is located in the gap between nanoparticles. The size of the gap is precisely controlled on the nanometer scale by tuning the Ag shell thickness. The EF of GSND with a 5 nm Ag shell is 2.7×10^{12} and ensures a yield of 73%. Li et al. [45] achieved SM-SERS with a nanoparticle-on-mirror (NPoM) (Figure 2b) [46,47] configuration, in which the gap between the nanoparticle and the metallic surface is determined by the length of the adsorbed molecules. The configuration could detect a distinguishable signal in 10 nM and achieve single-molecule sensitivity as proven by the bianalyte approach. Further, Carnegie et al. [48] observed the optically induced formation of picocavities in NPoM, which further focused the local field down to the subnanometer scale. The picocavities were stabilized at room temperature by chemically modifying the self-assembled monolayers. When SERS is combined with nonlinear optical processes, such as stimulated Raman spectroscopy (SRS) and coherent anti-Stokes Raman scattering (CARS), more complex nanostructures are utilized [49]. Zhang et al. [50] demonstrated a Fano-resonant quadrumer substrate (Figure 2c) to achieve single-molecule surface-enhanced CARS. Pump light, Stokes scattering, and anti-Stokes scattering are simultaneously enhanced with the quadrumer substrate. An EF of 10^{11} over spontaneous Raman scattering was realized, which is capable of single-molecule detection.

DNA origami [51], a powerful nanoengineering tool, offers an elegant approach to designing sophisticated nanostructures. In DNA origami, a long scaffold single strand and a set of short artificial staple strands are self-assembled in various 2D and 3D structures. Thacker et al. [52] assembled two 40 nm Au nanoparticles with gaps of 3.3 ± 1 nm on a DNA origami platform. The innovative structure ensures ultra-high EF between nanoparticles without occupying the gaps between them. Further, a series of functional complicated nanostructures were assembled on DNA origami platform, including heterodimers [53], nanostar dimers [54], bowties [55], nanocavities [56], nanoforks [57] (Figure 2d), etc.

Tip-enhanced Raman spectroscopy (TERS) [58–60], an extension of SERS, enhances the Raman signal of the analyte on the substrate by a plasmonic tip. The apex of a tip with a high aspect ratio induces the lightning rod effect and localizes the electromagnetic field into a tightly confined space [61]. With a sophisticated mechanical system, precise coupling of the tip and plasmonic substrate enables much larger EF, similar to the NPoM. Zhang et al. [14] realized single-molecule TERS in an ultra-high vacuum and low temperature (Figure 2e). The plasmonic tip and substrate form a nanocavity. By spectrally matching the SPR of the nanocavity and the electronic transition of the molecule, both Raman excitation and emission are enhanced. The chemical mapping of a single molecule with subnanometer spatial resolution was achieved. Furthermore, nonlinear TERS pushed the spatial resolution down to 0.5 nm [62]. Two adjacent molecules of very similar structure with van der Waals contact can be distinguished. Although single-molecule TERS is typically implemented at cryogenic temperature, recently, several reports have shown that TERS can achieve single-molecule sensitivity at room temperature [48]. Park et al. [63] performed variable temperature (90–300 K) single-molecule TERS of malachite green. From temperature-dependent line narrowing and splitting, the ultrafast vibrational dephasing, conformational

heterogeneity, and intramolecular coupling were quantified. Liu et al. [64] proposed fishing-mode TERS (FM-TERS) to study single-molecule junctions in different conduction states (Figure 2f). A bias voltage is applied between the tip and substrate to tune the conduction states of the single-molecule junction. Single-molecule conductance and Raman spectrum are simultaneously acquired at room temperature by FM-TERS.

Limited by the optical diffraction limit, the focal spot of the excitation beam is much larger than the hotspot. Improving coupling efficiency from far-field to near-field is a complementary approach to increase EF. Ahmed et al. [65] proposed a nanoantenna for directional SM-SERS. Wang et al. [66] fabricated a nanoantenna chip containing more than 10^3 nanoantennas with top-down fabrication methods (Figure 2g). Each nanoantenna consists of a Ag dimer with a 5 nm gap and a Ag ring, all on a SiO₂ spacer layer on a Ag mirror. The Ag mirror supports the SPR excited on the dimer, and the Ag ring converges the surface plasmon polaritons (SPPs) on the mirror to the dimer. The Ag mirror and Ag ring provide an extra two orders of magnitude EF. Chen et al. [15] demonstrated a plasmonic device consisting of a sub-10 nm wide and 1 μ m long nanoslit, a cavity, and two Bragg-mirror gratings for single-molecule nucleobase sensing (Figure 2h). The cavity efficiently couples the excitation light into SPPs and guides them into the nanoslit. Two Bragg-mirror gratings reflect SPPs back into the slit-cavity to further strengthen the enhanced field. In TERS, a spiral tip fabricated by metal deposition and direct laser writing is proposed [67,68]. Through the spiral design, the mirror symmetry of the plasmonic tip is broken, avoiding destructive interference of the coupled SPPs, achieving 30% greater EM enhancement than the conical tip.

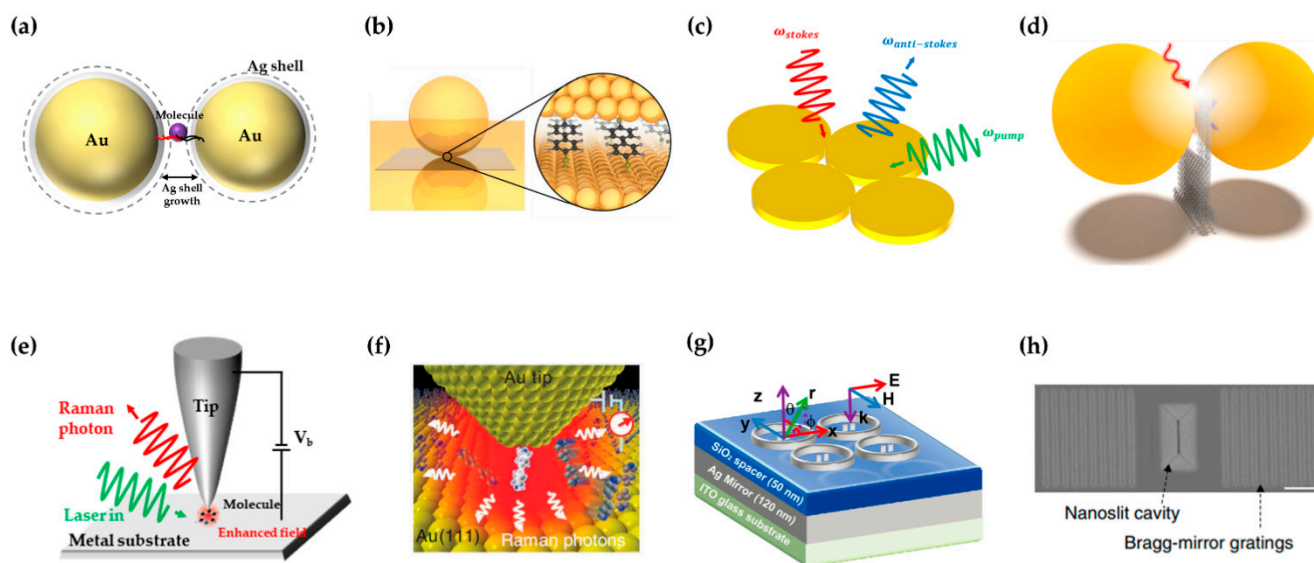


Figure 2. High-reproducibility substrates for SM-SERS. (a) Nanogap-engineered SERS-active GSND. (b) NPoM configuration. Figure reproduced from [46]. (c) The enhancement map of the quadrumer substrate. (d) Nanoparticle dimer assembled on the DNA origami nanofork. Figure reproduced from [57]. (e) Tunneling-controlled TERS. (f) Schematic diagram of FM-TERS. Figure reproduced from [64]. (g) Nanoantenna chip for SM-SERS. Figure reproduced from [66]. (h) The SEM image of the nanoslit device. Scale bar, 1 μ m. Scanning electron microscopy, SEM. Figure reproduced from [15].

Reproducible SM-SERS experiments and data rely on the plasmonic nanogap with precise size control. So far, fabricating such a precise nanostructure is still a challenge in a variety of environments.

3.2. Strategies for Improving the Probability of Molecules in Hotspots

As mentioned above, in SM-SERS experiments based on random adsorption, it is a rare event that molecules are located in hotspots due to ultra-low concentration and

narrow hotspots with sparse distribution. Long observation time is required for statistical confidence, suffering from free diffusion of molecules. An approach is to chemically bind the molecule into the gap. In TERS, the hotspot generated by the tip is scanned along the substrate with scanning probe microscopy (SPM). All of the analytes on the substrate are present in the hotspot in one scan. However, single-molecule TERS is still limited by environment and imaging speed.

Expanding the volume of hotspots directly improves the probability of molecules in hotspots. Langmuir–Blodgett assembly is a powerful technique for assembling a large-area monolayer of anisotropic blocks [69]. Tao et al. [70] assembled Langmuir–Blodgett monolayers of aligned Ag nanowires covering over 20 cm² as a SERS substrate. Zhang et al. [71] reported a wrinkled, nanoporous Au film containing a high density of hotspots with EF of 10⁹. Mao et al. [72] designed a warped substrate instead of a flat substrate for NPoM by transformation optics, resulting in broadband enhancement in both magnitude and volume (Figure 3a). Single-molecule detection with only 60 s soaking time was achieved.

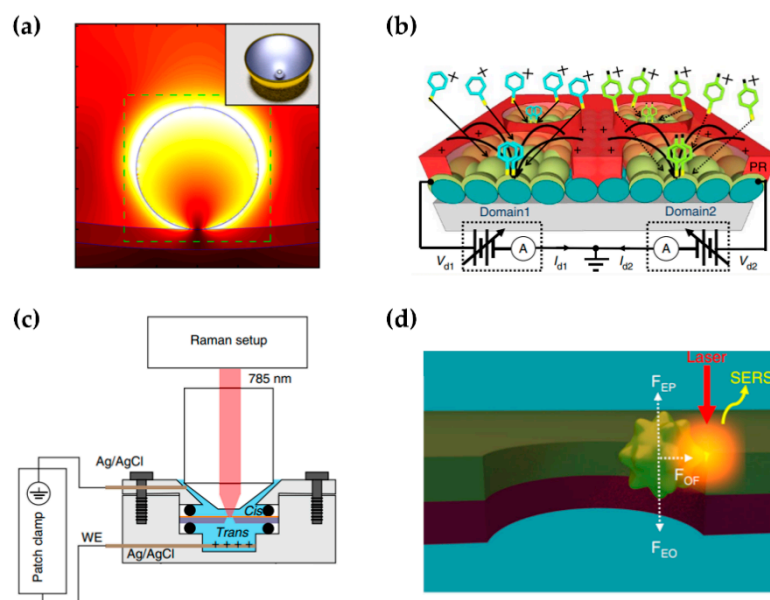


Figure 3. Strategies to improve the probability of molecules in hotspots. (a) FDTD simulation for a Ag nanoparticle on a warped Au substrate. Figure reproduced from [72]. Inset: the schematic of the NPoM with warped substrate. FDTD, finite difference time domain. (b) The SERS substrate with programmable localized electrodynamic precipitation. Figure reproduced from [73]. PR, patterned photoresist layer. (c) Schematic of the setup for nanoslit SERS. Figure reproduced from [15]. WE, working electrode. (d) Electro–plasmonic trapping due to the balance between the electrophoretic (F_{EP}), electroosmotic (F_{EO}), and plasmonic gradient force (F_{OF}). Figure reproduced from [74].

Another approach is to deliver molecules to the hotspots instead of random adsorption. Lin et al. [73] proposed a SERS substrate with programmable localized electrodynamic precipitation (Figure 3b). By applying a bias voltage to the substrate, analytes as far as centimeters away can be directed to the hotspots. Chen et al. [15] separated the electrolyte solution into two chambers by a nanoslit chip (Figure 3c). By applying a positive bias voltage, the nanoslit provides the only path from the cis to the trans chamber. Adsorption and translocation of molecules is manipulated by modulating the transmembrane voltage to match the slow sampling speed of SERS. Huang et al. [74] trapped the analyte molecules adsorbed on Au nanoparticles to the sidewall of a nanopore for minutes through a combination of electroosmotic force, electrophoretic force, and plasmonic gradient force (Figure 3d). In addition, localized optical heating, plasmonic optical trapping, and magnetic wells have been used for single-molecule manipulation in nanopore-based systems [75–77].

3.3. Nonmetallic and Hybrid Substrate

Conventional SERS substrates are dominated by noble metals, such as Au and Ag. However, Au and Ag typically suffer from high cost, heterogeneity, lack of stability, and bio-incompatibility. Nonmetallic materials, such as semiconductors, insulators, organic materials and 2D materials [78,79], can serve as alternatives or as complements to noble metal substrates. A range of nonmetallic SERS substrates has been proposed based on different principles, including total internal reflection [80], interference [81], optical amplification [82], Mie resonance [83], charge-transfer resonance [84], etc. CM is a common strategy for nonmetallic SERS substrates. However, CM-induced enhancement is relatively low; thus reports of SM-SERS with nonmetallic substrate are relatively rare.

Cong et al. [85] reported a sea urchin-like $W_{18}O_{49}$ nanowire as a SERS substrate, and realized a detection limit concentration of 10^{-7} M and EF of 3.4×10^5 . The oxygen deficiencies strengthen the substrate–analyte interactions and enable significant Raman enhancement. Keshavarz et al. [86] proposed a Si@SiO₂ quantum probe as a SERS probe for biomolecular and intracellular sensing due to its chemical stability and biocompatibility. Superior EF of 10^7 at pM concentration was achieved. On the other hand, a combination of metal and nonmetal has also been adopted for SM-SERS. CM-induced enhancement can relax requirement on EM-induced enhancement. He et al. [87] coupled Ag nanoparticles with Si nanowires to achieve an EF of 10^{10} . Shell-isolated nanoparticle-enhanced Raman spectroscopy (SHINERS) [88], coating Au nanoparticles with ultra-thin and pinhole-free Si shells, eliminated the influence of adsorbing analytes and has been widely used to investigate chemical reactions. In summary, it is still a challenge to develop nonmetallic substrates with single-molecule sensitivity to extend SM-SERS to more applications.

4. Application of SM-SERS

4.1. In Situ Monitoring of Catalytic Reactions

The rational design of highly efficient catalysts depends on understanding the structure–activity relationship and reaction mechanism at the single-molecule level. SM-SERS, with its ultra-high surface sensitivity, is a powerful tool for in situ monitoring and elucidating the mechanisms of catalytic reactions [89–92].

Noble metal nanoparticles can act as catalysts on which plasmon-induced hot electrons are transferred to reactants [93]. Zhang et al. [94] discovered a new plasmon catalyzed reaction of p-nitrothiophenol (pNTP) by SM-SERS. In previous studies, dimerization of pNTP to 4,4-dimercaptoazobenzene (DMAB) was thought to occur on the surface of Au nanoparticles. Nevertheless, dissociation of pNTP to thiophenol (TP) was observed at an ultra-low concentration (10^{-9} M), and plasmon-induced hot electrons provided the activation energy for the dissociation. Zhang et al. [95] reported direct SERS tracking of the catalytic reactions at a 13 nm Au nanoparticle. Spatially isolated Au dimers, consisting of two nanoparticles sized 200 nm and 13 nm, integrate catalytic activity and SERS into a single entity (Figure 4a). Further, combining SM-SERS with electrochemistry could drive the reactions by applying the bias voltage to inject or extract electrons from the analytes [64]. Nijs et al. [96] studied hot-electron reduction and oxidation dynamically with a NPoM configuration by SM-SERS (Figure 4b).

Generally, the catalytic activity of noble metals is relatively low. To expand SERS to a catalytically active transition metal, Tian et al. [97] employed Au nanoparticles coated with ultra-thin shells of a transition metal such as Pt, Pd, Ni, or Co. In such a scheme, the Raman signal of analytes adsorbed on the transition metal shell is enhanced by the Au core. SHINERS [88], already mentioned in the previous section, improve the chemical and thermal stability of the noble metal core, enabling in situ monitoring of catalytic reactions in harsh conditions (Figure 4c).

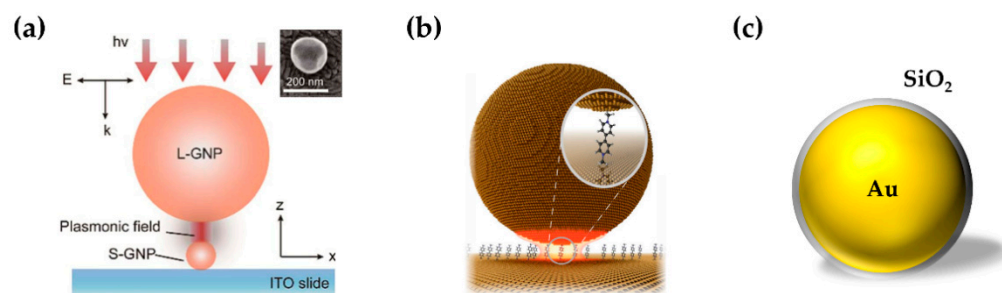


Figure 4. Monitoring of catalytic reactions by SM-SERS. (a) The Au dimers, consisting of two nanoparticles sized 200 nm and 13 nm. Figure reproduced from [95]. Inset: an SEM image of the Au dimers. L-GNP, large gold nanoparticles. S-GNP, small gold nanoparticles. ITO, indium tin oxide. (b) Self-assembled 80 nm NPoM for eliciting EF for SM-SERS. Figure reproduced from [96]. (c) SHINERS, Au core SiO₂ shell nanoparticles.

4.2. Characterization of Molecular Nanoelectronics

Molecular nanoelectronics use single molecules as building blocks of logic units, electronic devices, and circuits, with small size, low power consumption, and unconventional properties [98]. However, poor reproducibility limits the application of molecular nanoelectronics. The molecular structure in nanoelectronic devices is not clear by conventional conductance measurements [99]. SM-SERS, as a complementary characterization method, could study molecular conformation and metal–molecule interface structure and charge transfer at room temperature.

Liu et al. [64] observed voltage-dependent peak splitting due to the different bonding interactions occurring on the Au–4bipy–Au junction (4,4′-bipyridine, 4bipy) by FM-TERS (Figure 5a). Kaneko et al. [100] studied the selectivity of adsorption sites in a single-molecule junction by simultaneous SERS and conductance measurements (Figure 5b). The conductance response revealed the coexistence of three metastable states in 1,4-benzenedithiol (BDT) junctions. The SERS results showed selectivity of adsorption site toward “bridge sites”. Han et al. [101] studied the influence of SPR on interfacial charge transfer in TiO₂–MBA–Au assemblies (MBA, mercaptobenzoic acid) by SERS. Li et al. [102] studied voltage tuning of vibrational mode in C₆₀ junctions (Figure 5c). Applying a bias to the junction, vibrational mode softening approximately quadratic in the bias voltage occurs. This stark effect alone cannot explain the phenomenon, but alteration of the molecular charge state is responsible for the effect.

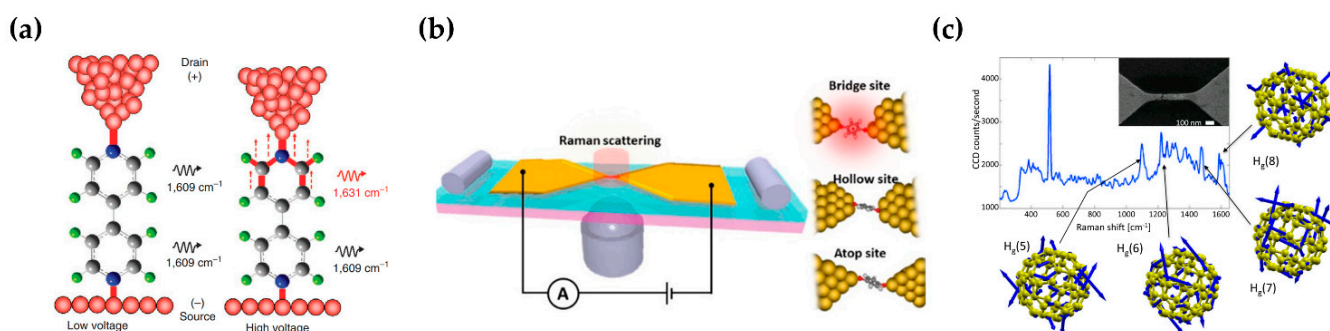


Figure 5. Characterization of molecular nanoelectronics by SM-SERS. (a) The schematic of the Au–4bipy–Au junction with low/high bias voltage. Figure reproduced from [64]. (b) Simultaneous SERS and conductance measurements for single-molecule junction. Figure reproduced from [100]. Right: three metastable states in BDT junctions. (c) SERS of C₆₀ in an electromigrated junction. Figure reproduced from [102]. Inset: an SEM image of an electromigrated junction.

4.3. Single-Molecule Sensing

Single-molecule sensing is an important subject in biochemical analysis. In single-molecule sensing, observation of each molecule is an independent event, revealing information that is drowned out by statistical average, such as sample heterogeneity, molecular mechanism, and complex kinetic rate [8]. For fluorescence or conductance measurements, one-dimensional data provide limited information that different molecules may yield similar signals. SM-SERS provides rich spectral information conducive to distinguishing a variety of similar analytes [75,103,104], which is of great significance in DNA sequencing, protein identification, etc. Further, Zhou et al. [105] utilized the rich spectral information to probe the orientation and oxygenation of single molecules.

TERS can achieve both single-molecule sensitivity and subnanometer spatial resolution. After depositing the analytes on the substrate, the chemical structure of single molecules can be imaged [14,62]. Viruses [106], single-stranded DNA [107], and RNA [108] have been identified by single-molecule TERS (Figure 6a).

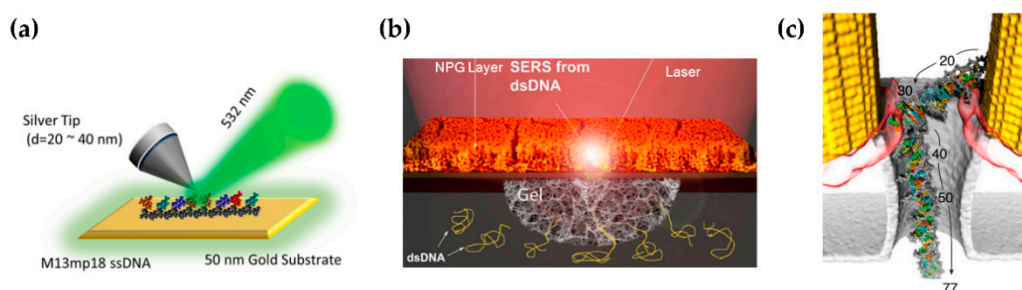


Figure 6. Biochemical sensing by SM-SERS. (a) Identification of single-stranded DNA by single-molecule TERS. Figure reproduced from [107]. The DNA molecules are deposited on the Au substrate. (b) The schematic of the plasmonic nanopore in the nanoporous film. NPG, nanoporous gold. Figure reproduced from [109]. (c) DNA sequence trapped in plasmonic nanopore. The base pairs are numbered in ascending order from tail to front of the molecule. Figure reproduced from [110].

A plasmonic nanopore is a single-molecule sensor widely used in solution at room temperature. The electrolyte solution is divided into two chambers by an electrically insulating membrane on which the nanopore is a nanoscale aperture. A bias voltage applied across the membrane drives the charged analyte through the nanopore [111]. The ionic current and SERS signal are detected when the analytes pass through the nanopore, which can be used for single-molecule sensing. Translocation of amino acids, nucleobases, and DNA has been probed through plasmonic nanopores [112,113]. Nevertheless, in SERS measurement based on nanopores, translocation time is on the order of microseconds, which is insufficient for the spectrum acquisition on the order of milliseconds. Zong et al. [114] utilized dynamic SERS to improve the signal-to-noise ratio (SNR) even when the acquisition time cannot catch up with the diffusion time of molecules. With insufficient acquisition time, SERS was extracted via data processing from time-dependent spectral series. Hubarevich et al. [109] fabricated a plasmonic nanopore in a thick nanoporous film and added hydrogel at the bottom of the nanoporous membrane, which significantly reduced the velocity of translocation (Figure 6b). Single-molecule trapping has been adopted to prolong the residence time of molecules within nanopores [15,74–77], as described in Section 3.2. Although a series of single molecules have been identified in nanopore by SM-SERS, more delicate operations, such as stepwise displacement of DNA strands through the nanopore, have not been realized in experiments (Figure 6c) [110].

5. Several Challenges in SM-SERS

As mentioned in the previous sections, with vigorous development in recent years, SM-SERS has achieved great success in various fields. However, SM-SERS has not been fully developed yet. Several challenges still need to be overcome to further boost advancement.

First, although EM and CM have explained a lot of SERS phenomena in the past two decades, some experimental events are still confusing. Indeed, the mechanism of SERS is not completely clear, especially for single-molecule events. It has been proposed that some previously ignored physical effects such as Rayleigh scattering, discrete interaction, and quantum interaction deserve to be considered in the mechanism [23–26]. Thus, it is necessary to extend the SERS theory to take physical effects into account. Further, the extended SERS theory can also provide insights into the design of advanced SERS systems.

Second, the intrinsic fluctuation of SM-SERS disturbs the data analysis algorithm, but on the other hand also implies single-molecule information. An algorithm for extracting single-molecule chemical information from SM-SERS data has not been developed. The study of spectral fluctuation and blinking could deepen the understanding of SM-SERS data and develop advanced data analysis algorithm for SM-SERS.

Third, in airborne environments and solutions at room temperature, the reproducibility of SM-SERS experiments is still poor, which is attributed to two aspects. On the one hand, the Brownian motion of molecules in the hotspot induces spectral fluctuations. Delicate single-molecule manipulation techniques are required to localize molecules to the same position of the hotspot or even drive molecules stepwise through the hotspot [110,115,116]. On the other hand, fabrication of SM-SERS substrates is also important to obtain high-reproducibility substrates.

Fourth, nonmetallic substrates greatly broaden the application of SERS. However, due to the poor SERS activity of nonmetal, nonmetallic substrates with single-molecule sensitivity have rarely been reported. Material structural and hotspot engineering may lead to the development of SM-SERS with nonmetallic substrates [78].

Fifth, ultrafast SERS, incorporating SERS with an ultrafast technique, has opened a new direction due to its fs and ps time resolution and higher sensitivity [49,117]. Ultrafast SERS can provide real-time monitoring of molecular structure and bond breaking and forming, enabling elucidation of mechanisms of plasmon-induced photochemical and photophysical processes.

6. Conclusions

In this review, we first elucidate the key concepts of SM-SERS, including EF, spectral fluctuation, and experimental evidence of single-molecule events. Next, we systematically discuss advanced implementations of SM-SERS, including substrates with ultra-high EF and reproducibility, strategies to improve the probability of molecules in hotspots, and nonmetallic and hybrid substrates. Then, several examples for the application of SM-SERS are proposed, including catalysis, nanoelectronics, and sensing. Finally, we summarize the challenges and future of SM-SERS. We hope this literature review will inspire the interest of researchers in more fields. SM-SERS is expected to make more progress in science and application in the near future.

Author Contributions: Conceptualization, L.T. and X.L.; methodology, L.T. and C.K.; validation, L.T.; investigation, L.T. and Y.Q.; writing-original draft preparation, Y.Q.; writing-review and editing, L.T. and Y.Q.; supervision, X.L., L.T. and C.K.; funding acquisition, L.T. and C.K. All authors have read and agreed to the published version of the manuscript.

Funding: This research was funded by the Natural Science Foundation of Zhejiang Province (grant no. LR22F050003), National Natural Science Foundation of China (grant no. 21874119, 62125504, 62127818), the National Key R&D Program of China (grant no. 2020YFC2004600) and Zhejiang Provincial Ten Thousand Plan for Young Top Talents (grant no. 2020R52001).

Institutional Review Board Statement: Not applicable.

Informed Consent Statement: Not applicable.

Data Availability Statement: Not applicable.

Conflicts of Interest: The authors declare no conflict of interest.

References

1. Raman, C.V.; Krishnan, K.S. A new type of secondary radiation. *Nature* **1928**, *121*, 501–502. [[CrossRef](#)]
2. Hanlon, E.B.; Manoharan, R.; Koo, T.W.; Shafer, K.E.; Motz, J.T.; Fitzmaurice, M.; Kramer, J.R.; Itzkan, I.; Dasari, R.R.; Feld, M.S. Prospects for in vivo Raman spectroscopy. *Phys. Med. Biol.* **2000**, *45*, R1. [[CrossRef](#)] [[PubMed](#)]
3. Fleischmann, M.; Hendra, P.J.; McQuillan, A.J. Raman-spectra of pyridine adsorbed at a silver electrode. *Chem. Phys. Lett.* **1974**, *26*, 163–166. [[CrossRef](#)]
4. Guerrini, L.; Graham, D. Molecularly-mediated assemblies of plasmonic nanoparticles for Surface-Enhanced Raman Spectroscopy applications. *Chem. Soc. Rev.* **2012**, *41*, 7085–7107. [[CrossRef](#)]
5. Yamamoto, Y.S.; Itoh, T. Why and how do the shapes of surface-enhanced Raman scattering spectra change? Recent progress from mechanistic studies. *J. Raman Spectrosc.* **2016**, *47*, 78–88. [[CrossRef](#)]
6. Ding, S.Y.; Yi, J.; Li, J.F.; Ren, B.; Wu, D.Y.; Panneerselvam, R.; Tian, Z.Q. Nanostructure-based plasmon-enhanced Raman spectroscopy for surface analysis of materials. *Nat. Rev. Mater.* **2016**, *1*, 16021. [[CrossRef](#)]
7. Kiguchi, M.; Aiba, A.; Fujii, S.; Kobayashi, S. Surface enhanced Raman scattering on molecule junction. *Appl. Mater. Today* **2019**, *14*, 76–83. [[CrossRef](#)]
8. Spitzberg, J.D.; Zreben, A.; van Kooten, X.F.; Meller, A. Plasmonic-nanopore biosensors for superior single-molecule detection. *Adv. Mater.* **2019**, *31*, 1900422. [[CrossRef](#)]
9. Yu, Y.; Xiao, T.H.; Wu, Y.Z.; Li, W.J.; Zeng, Q.G.; Long, L.; Li, Z.Y. Roadmap for single-molecule surface-enhanced Raman spectroscopy. *Adv. Photonics* **2020**, *2*, 014002. [[CrossRef](#)]
10. Kneipp, K.; Wang, Y.; Kneipp, H.; Perelman, L.T.; Itzkan, I.; Dasari, R.; Feld, M.S. Single molecule detection using surface-enhanced Raman scattering (SERS). *Phys. Rev. Lett.* **1997**, *78*, 1667–1670. [[CrossRef](#)]
11. Nie, S.M.; Emery, S.R. Probing single molecules and single nanoparticles by surface-enhanced Raman scattering. *Science* **1997**, *275*, 1102–1106. [[CrossRef](#)] [[PubMed](#)]
12. Claridge, S.A.; Schwartz, J.J.; Weiss, P.S. Electrons, photons, and force: Quantitative single-molecule measurements from physics to biology. *ACS Nano* **2011**, *5*, 693–729. [[CrossRef](#)] [[PubMed](#)]
13. Tang, L.H.; Nadappuram, B.P.; Cadinu, P.; Zhao, Z.Y.; Xue, L.; Yi, L.; Ren, R.; Wang, J.W.; Ivanov, A.P.; Edel, J.B. Combined quantum tunnelling and dielectrophoretic trapping for molecular analysis at ultra-low analyte concentrations. *Nat. Commun.* **2021**, *12*, 913. [[CrossRef](#)] [[PubMed](#)]
14. Zhang, R.; Zhang, Y.; Dong, Z.C.; Jiang, S.; Zhang, C.; Chen, L.G.; Zhang, L.; Liao, Y.; Aizpurua, J.; Luo, Y.; et al. Chemical mapping of a single molecule by plasmon-enhanced Raman scattering. *Nature* **2013**, *498*, 82–86. [[CrossRef](#)]
15. Chen, C.; Li, Y.; Kerman, S.; Neutens, P.; Willems, K.; Cornelissen, S.; Lagae, L.; Stakenborg, T.; Van Dorpe, P. High spatial resolution nanoslit SERS for single-molecule nucleobase sensing. *Nat. Commun.* **2018**, *9*, 1733. [[CrossRef](#)]
16. Kleinman, S.L.; Frontiera, R.R.; Henry, A.I.; Dieringer, J.A.; Van Duyne, R.P. Creating, characterizing, and controlling chemistry with SERS hot spots. *Phys. Chem. Chem. Phys.* **2013**, *15*, 21–36. [[CrossRef](#)]
17. Li, Z.Y. Mesoscopic and microscopic strategies for engineering plasmon-enhanced Raman scattering. *Adv. Opt. Mater.* **2018**, *6*, 1701097. [[CrossRef](#)]
18. Pieczonka, N.P.W.; Aroca, R.F. Single molecule analysis by surface-enhanced Raman scattering. *Chem. Soc. Rev.* **2008**, *37*, 946–954. [[CrossRef](#)]
19. Shim, S.; Stuart, C.M.; Mathies, R.A. Resonance Raman cross-sections and vibronic analysis of rhodamine 6G from broadband stimulated Raman spectroscopy. *Chemphyschem* **2008**, *9*, 697–699. [[CrossRef](#)]
20. Blackie, E.J.; Le Ru, E.C.; Etchegoin, P.G. Single-molecule surface-enhanced Raman spectroscopy of nonresonant molecules. *J. Am. Chem. Soc.* **2009**, *131*, 14466–14472. [[CrossRef](#)]
21. Morris, M.D. Resonance Raman spectroscopy—current applications and prospects. *Anal. Chem.* **1979**, *51*, 182. [[CrossRef](#)]
22. Etchegoin, P.G.; Le Ru, E.C. A perspective on single molecule SERS: Current status and future challenges. *Phys. Chem. Chem. Phys.* **2008**, *10*, 6079–6089. [[CrossRef](#)] [[PubMed](#)]
23. Zhang, C.; Chen, B.Q.; Li, Z.Y. Optical origin of subnanometer resolution in tip-enhanced Raman mapping. *J. Phys. Chem. C* **2015**, *119*, 11858–11871. [[CrossRef](#)]
24. Fiederling, K.; Abasifard, M.; Richter, M.; Deckert, V.; Graefe, S.; Kupfer, S. The chemical effect goes resonant—a full quantum mechanical approach on TERS. *Nanoscale* **2020**, *12*, 6346–6359. [[CrossRef](#)] [[PubMed](#)]
25. Fiederling, K.; Kupfer, S.; Grafe, S. Are charged tips driving TERS-resolution? A full quantum chemical approach. *J. Chem. Phys.* **2021**, *154*, 034106. [[CrossRef](#)] [[PubMed](#)]
26. Morton, S.M.; Jensen, L. A discrete interaction model/quantum mechanical method to describe the interaction of metal nanoparticles and molecular absorption. *J. Chem. Phys.* **2011**, *135*, 134103. [[CrossRef](#)]
27. Le Ru, E.C.; Etchegoin, P.G.; Meyer, M. Enhancement factor distribution around a single surface-enhanced Raman scattering hot spot and its relation to single molecule detection. *J. Chem. Phys.* **2006**, *125*, 204701. [[CrossRef](#)]
28. Dieringer, J.A.; Lettan, R.B.; Scheidt, K.A.; Van Duyne, R.P. A frequency domain existence proof of single-molecule surface-enhanced Raman Spectroscopy. *J. Am. Chem. Soc.* **2007**, *129*, 16249–16256. [[CrossRef](#)]
29. Zrimsek, A.B.; Chiang, N.H.; Mattei, M.; Zaleski, S.; McAnally, M.O.; Chapman, C.T.; Henry, A.I.; Schatz, G.C.; Van Duyne, R.P. Single-molecule chemistry with surface- and tip-enhanced Raman spectroscopy. *Chem. Rev.* **2017**, *117*, 7583–7613. [[CrossRef](#)]

30. Le Ru, E.C.; Meyer, M.; Etchegoin, P.G. Proof of single-molecule sensitivity in surface enhanced Raman scattering (SERS) by means of a two-analyte technique. *J. Phys. Chem. B* **2006**, *110*, 1944–1948. [[CrossRef](#)]
31. Lahr, R.H.; Vikesland, P.J. Surface-enhanced Raman spectroscopy (SERS) cellular imaging of intracellular biosynthesized gold nanoparticles. *ACS Sustain. Chem. Eng.* **2014**, *2*, 1599–1608. [[CrossRef](#)]
32. Fang, Z.; Wang, W.; Lu, A.X.; Wu, Y.; Liu, Y.; Yan, C.C.; Han, C.Q. Rapid classification of honey varieties by surface enhanced Raman scattering combining with deep learning. In Proceedings of the Cross Strait Quad-Regional Radio Science and Wireless Technology Conference (CSQRWC), Xuzhou, China, 21–24 July 2018.
33. Zhang, R.; Xie, H.M.; Cai, S.N.; Hu, Y.; Liu, G.K.; Hong, W.J.; Tian, Z.Q. Transfer-learning-based Raman spectra identification. *J. Raman Spectrosc.* **2020**, *51*, 176–186. [[CrossRef](#)]
34. Lindquist, N.C.; de Albuquerque, C.D.L.; Sobral-Filho, R.G.; Paci, I.; Brolo, A.G. High-speed imaging of surface-enhanced Raman scattering fluctuations from individual nanoparticles. *Nat. Nanotechnol.* **2019**, *14*, 981. [[CrossRef](#)] [[PubMed](#)]
35. Kudelski, A.; Pettinger, B. Fluctuations of surface-enhanced Raman spectra of CO adsorbed on gold substrates. *Chem. Phys. Lett.* **2004**, *383*, 76–79. [[CrossRef](#)]
36. Marshall, A.R.L.; Stokes, J.; Viscomi, F.N.; Proctor, J.E.; Gierschner, J.; Bouillard, J.S.G.; Adawi, A.M. Determining molecular orientation via single molecule SERS in a plasmonic nano-gap. *Nanoscale* **2017**, *9*, 17415–17421. [[CrossRef](#)] [[PubMed](#)]
37. Weber, M.L.; Willets, K.A. Correlated super-resolution optical and structural studies of surface-enhanced Raman scattering hot spots in silver colloid aggregates. *J. Phys. Chem. Lett.* **2011**, *2*, 1766–1770. [[CrossRef](#)]
38. Maruyama, Y.; Ishikawa, M.; Futamata, M. Thermal activation of blinking in SERS signal. *J. Phys. Chem. B* **2004**, *108*, 673–678. [[CrossRef](#)]
39. Galloway, C.M.; Le Ru, E.C.; Etchegoin, P.G. Single-molecule vibrational pumping in SERS. *Phys. Chem. Chem. Phys.* **2009**, *11*, 7372–7380. [[CrossRef](#)]
40. Emory, S.R.; Jensen, R.A.; Wenda, T.; Han, M.Y.; Nie, S.M. Re-examining the origins of spectral blinking in single-molecule and single-nanoparticle SERS. *Faraday Discuss.* **2006**, *132*, 249–259. [[CrossRef](#)]
41. Haran, G. Single molecule Raman spectroscopy and local work function fluctuations. *Isr. J. Chem.* **2004**, *44*, 385–390. [[CrossRef](#)]
42. Xu, H.X.; Bjerneld, E.J.; Kall, M.; Borjesson, L. Spectroscopy of single hemoglobin molecules by surface enhanced Raman scattering. *Phys. Rev. Lett.* **1999**, *83*, 4357–4360. [[CrossRef](#)]
43. Fang, Y.; Seong, N.H.; Dlott, D.D. Measurement of the distribution of site enhancements in surface-enhanced Raman scattering. *Science* **2008**, *321*, 388–392. [[CrossRef](#)] [[PubMed](#)]
44. Lim, D.K.; Jeon, K.S.; Kim, H.M.; Nam, J.M.; Suh, Y.D. Nanogap-engineerable Raman-active nanodumbbells for single-molecule detection. *Nat. Mater.* **2010**, *9*, 60–67. [[CrossRef](#)]
45. Li, L.; Hutter, T.; Steiner, U.; Mahajan, S. Single molecule SERS and detection of biomolecules with a single gold nanoparticle on a mirror junction. *Analyst* **2013**, *138*, 4574–4578. [[CrossRef](#)] [[PubMed](#)]
46. Benz, F.; Tserkezis, C.; Herrmann, L.O.; de Nijs, B.; Sanders, A.; Sigle, D.O.; Pukenas, L.; Evans, S.D.; Aizpurua, J.; Baumberg, J.J. Nanooptics of molecular-shunted plasmonic nanojunctions. *Nano Lett.* **2015**, *15*, 669–674. [[CrossRef](#)]
47. Huang, Y.; Ma, L.; Li, J.; Zhang, Z. Nanoparticle-on-mirror cavity modes for huge and/or tunable plasmonic field enhancement. *Nanotechnology* **2017**, *28*, 105203. [[CrossRef](#)]
48. Carnegie, C.; Griffiths, J.; de Nijs, B.; Readman, C.; Chikkaraddy, R.; Deacon, W.M.; Zhang, Y.; Szabo, I.; Rosta, E.; Aizpurua, J.; et al. Room-temperature optical picocavities below 1 nm³ accessing single-atom geometries. *J. Phys. Chem. Lett.* **2018**, *9*, 7146–7151. [[CrossRef](#)]
49. Gruenke, N.L.; Cardinal, M.F.; McAnally, M.O.; Frontiera, R.R.; Schatza, G.C.; Van Duyne, R.P. Ultrafast and nonlinear surface-enhanced Raman spectroscopy. *Chem. Soc. Rev.* **2016**, *45*, 2263–2290. [[CrossRef](#)]
50. Zhang, Y.; Zhen, Y.R.; Neumann, O.; Day, J.K.; Nordlander, P.; Halas, N.J. Coherent anti-Stokes Raman scattering with single-molecule sensitivity using a plasmonic Fano resonance. *Nat. Commun.* **2014**, *5*, 4424. [[CrossRef](#)]
51. Rothmund, P.W.K. Folding DNA to create nanoscale shapes and patterns. *Nature* **2006**, *440*, 297–302. [[CrossRef](#)]
52. Thacker, V.V.; Herrmann, L.O.; Sigle, D.O.; Zhang, T.; Liedl, T.; Baumberg, J.J.; Keyser, U.F. DNA origami based assembly of gold nanoparticle dimers for surface-enhanced Raman scattering. *Nat. Commun.* **2014**, *5*, 3448. [[CrossRef](#)] [[PubMed](#)]
53. Weller, L.; Thacker, V.V.; Herrmann, L.O.; Hemmig, E.A.; Lombardi, A.; Keyser, U.F.; Baumberg, J.J. Gap-dependent coupling of Ag-Au nanoparticle heterodimers using DNA origami-based self-assembly. *ACS Photonics* **2016**, *3*, 1589–1595. [[CrossRef](#)]
54. Tanwar, S.; Haldar, K.K.; Sen, T. DNA origami directed Au nanostar dimers for single-molecule surface-enhanced Raman scattering. *J. Am. Chem. Soc.* **2017**, *139*, 17639–17648. [[CrossRef](#)] [[PubMed](#)]
55. Zhan, P.F.; Wen, T.; Wang, Z.G.; He, Y.B.; Shi, J.; Wang, T.; Liu, X.F.; Lu, G.W.; Ding, B.Q. DNA origami directed assembly of gold bowtie nanoantennas for single-molecule surface-enhanced Raman scattering. *Angew. Chem. Int. Ed.* **2018**, *57*, 2846–2850. [[CrossRef](#)]
56. Chikkaraddy, R.; Turek, V.A.; Kongsuwan, N.; Benz, F.; Carnegie, C.; van de Goor, T.; de Nijs, B.; Demetriadou, A.; Hess, O.; Keyser, U.F.; et al. Mapping nanoscale hotspots with single-molecule emitters assembled into plasmonic nanocavities using DNA origami. *Nano Lett.* **2018**, *18*, 405–411. [[CrossRef](#)] [[PubMed](#)]
57. Tapio, K.; Mostafa, A.; Kanehira, Y.; Suma, A.; Dutta, A.; Bald, I. A versatile DNA origami-based plasmonic nanoantenna for label-free single-molecule surface-enhanced Raman spectroscopy. *ACS Nano* **2021**, *15*, 7065–7077. [[CrossRef](#)]

58. Stockle, R.M.; Suh, Y.D.; Deckert, V.; Zenobi, R. Nanoscale chemical analysis by tip-enhanced Raman spectroscopy. *Chem. Phys. Lett.* **2000**, *318*, 131–136. [[CrossRef](#)]
59. Vasconcelos, T.L.; Archanjo, B.S.; Fragneaud, B.; Oliveira, B.S.; Riikonen, J.; Li, C.F.; Ribeiro, D.S.; Rabelo, C.; Rodrigues, W.N.; Jorio, A.; et al. Tuning localized surface plasmon resonance in scanning near-field optical microscopy probes. *ACS Nano* **2015**, *9*, 6297–6304. [[CrossRef](#)]
60. Jaculbia, R.B.; Imada, H.; Miwa, K.; Iwasa, T.; Takenaka, M.; Yang, B.; Kazuma, E.; Hayazawa, N.; Taketsugu, T.; Kim, Y. Single-molecule resonance Raman effect in a plasmonic nanocavity. *Nat. Nanotechnol.* **2020**, *15*, 105. [[CrossRef](#)]
61. Verma, P. Tip-enhanced Raman spectroscopy: Technique and recent advances. *Chem. Rev.* **2017**, *117*, 6447–6466. [[CrossRef](#)]
62. Jiang, S.; Zhang, Y.; Zhang, R.; Hu, C.R.; Liao, M.H.; Luo, Y.; Yang, J.L.; Dong, Z.C.; Hou, J.G. Distinguishing adjacent molecules on a surface using plasmon-enhanced Raman scattering. *Nat. Nanotechnol.* **2015**, *10*, 865–869. [[CrossRef](#)] [[PubMed](#)]
63. Park, K.D.; Muller, E.A.; Kravtsov, V.; Sass, P.M.; Dreyer, J.; Atkin, J.M.; Raschke, M.B. Variable-temperature tip-enhanced Raman spectroscopy of single-molecule fluctuations and dynamics. *Nano Lett.* **2016**, *16*, 479–487. [[CrossRef](#)] [[PubMed](#)]
64. Liu, Z.; Ding, S.Y.; Chen, Z.B.; Wang, X.; Tian, J.H.; Anema, J.R.; Zhou, X.S.; Wu, D.Y.; Mao, B.W.; Xu, X.; et al. Revealing the molecular structure of single-molecule junctions in different conductance states by fishing-mode tip-enhanced Raman spectroscopy. *Nat. Commun.* **2011**, *2*, 305. [[CrossRef](#)] [[PubMed](#)]
65. Ahmed, A.; Gordon, R. Single molecule directivity enhanced Raman scattering using nanoantennas. *Nano Lett.* **2012**, *12*, 2625–2630. [[CrossRef](#)]
66. Wang, D.X.; Zhu, W.Q.; Best, M.D.; Camden, J.P.; Crozier, K.B. Directional Raman scattering from single molecules in the feed gaps of optical antennas. *Nano Lett.* **2013**, *13*, 2194–2198. [[CrossRef](#)]
67. Li, J.F.; Mu, J.J.; Wang, B.L.; Ding, W.; Liu, J.; Guo, H.L.; Li, W.X.; Gu, C.Z.; Li, Z.Y. Direct laser writing of symmetry-broken spiral tapers for polarization-insensitive three-dimensional plasmonic focusing. *Laser Photonics Rev.* **2014**, *8*, 602–609. [[CrossRef](#)]
68. Mu, J.J.; Liu, Z.G.; Li, J.F.; Hao, T.T.; Wang, Y.J.; Sun, S.S.; Li, Z.Y.; Li, J.J.; Li, W.X.; Gu, C.Z. Direct laser writing of pyramidal plasmonic structures with apertures and asymmetric gratings towards efficient subwavelength light focusing. *Opt. Express* **2015**, *23*, 22564–22571. [[CrossRef](#)]
69. Weekes, S.M.; Ogrin, F.Y.; Murray, W.A.; Keatley, P.S. Macroscopic arrays of magnetic nanostructures from self-assembled nanosphere templates. *Langmuir* **2007**, *23*, 1057–1060. [[CrossRef](#)]
70. Tao, A.; Kim, F.; Hess, C.; Goldberger, J.; He, R.R.; Sun, Y.G.; Xia, Y.N.; Yang, P.D. Langmuir-Blodgett silver nanowire monolayers for molecular sensing using surface-enhanced Raman spectroscopy. *Nano Lett.* **2003**, *3*, 1229–1233. [[CrossRef](#)]
71. Zhang, L.; Lang, X.Y.; Hirata, A.; Chen, M.W. Wrinkled nanoporous gold films with ultrahigh surface-enhanced Raman scattering enhancement. *ACS Nano* **2011**, *5*, 4407–4413. [[CrossRef](#)]
72. Mao, P.; Liu, C.X.; Favraud, G.; Chen, Q.; Han, M.; Fratallocchi, A.; Zhang, S. Broadband single molecule SERS detection designed by warped optical spaces. *Nat. Commun.* **2018**, *9*, 5428. [[CrossRef](#)] [[PubMed](#)]
73. Lin, E.C.; Fang, J.; Park, S.C.; Johnson, F.W.; Jacobs, H.O. Effective localized collection and identification of airborne species through electrodynamic precipitation and SERS-based detection. *Nat. Commun.* **2013**, *4*, 1636. [[CrossRef](#)] [[PubMed](#)]
74. Huang, J.A.; Mousavi, M.Z.; Zhao, Y.Q.; Hubarevich, A.; Omeis, F.; Giovannini, G.; Schutte, M.; Garoli, D.; De Angelis, F. SERS discrimination of single DNA bases in single oligonucleotides by electro-plasmonic trapping. *Nat. Commun.* **2019**, *10*, 5321. [[CrossRef](#)] [[PubMed](#)]
75. Garoli, D.; Yamazaki, H.; Maccaferri, N.; Wanunu, M. Plasmonic nanopores for single-molecule detection and manipulation: Toward sequencing applications. *Nano Lett.* **2019**, *19*, 7553–7562. [[CrossRef](#)] [[PubMed](#)]
76. Pang, Y.J.; Gordon, R. Optical trapping of a single protein. *Nano Lett.* **2012**, *12*, 402–406. [[CrossRef](#)] [[PubMed](#)]
77. Fotouhi, B.; Ahmadi, V.; Faramarzi, V. Nano-plasmonic-based structures for DNA sequencing. *Opt. Lett.* **2016**, *41*, 4229–4232. [[CrossRef](#)]
78. Alessandri, I.; Lombardi, J.R. Enhanced Raman scattering with dielectrics. *Chem. Rev.* **2016**, *116*, 14921–14981. [[CrossRef](#)]
79. Lin, W. A durable plastic substrate for surface-enhanced Raman spectroscopy. *Appl. Phys. Mater. Sci. Processing* **2011**, *102*, 121–125. [[CrossRef](#)]
80. Woods, D.A.; Bain, C.D. Total internal reflection Raman spectroscopy. *Analyst* **2012**, *137*, 35–48. [[CrossRef](#)]
81. Connell, G.A.N.; Nemanich, R.J.; Tsai, C.C. Interference enhanced Raman-scattering from very thin absorbing films. *Appl. Phys. Lett.* **1980**, *36*, 31–33. [[CrossRef](#)]
82. Alessandri, I. Enhancing Raman scattering without plasmons: Unprecedented sensitivity achieved by TiO₂ shell-based resonators. *J. Am. Chem. Soc.* **2013**, *135*, 5541–5544. [[CrossRef](#)] [[PubMed](#)]
83. Dmitriev, P.A.; Baranov, D.G.; Milichko, V.A.; Makarov, S.V.; Mukhin, I.S.; Samusev, A.K.; Krasnok, A.E.; Belov, P.A.; Kivshar, Y.S. Resonant Raman scattering from silicon nanoparticles enhanced by magnetic response. *Nanoscale* **2016**, *8*, 9721–9726. [[CrossRef](#)] [[PubMed](#)]
84. Zheng, Z.H.; Cong, S.; Gong, W.B.; Xuan, J.N.; Li, G.H.; Lu, W.B.; Geng, F.X.; Zhao, Z.G. Semiconductor SERS enhancement enabled by oxygen incorporation. *Nat. Commun.* **2017**, *8*, 1993. [[CrossRef](#)]
85. Cong, S.; Yuan, Y.Y.; Chen, Z.G.; Hou, J.Y.; Yang, M.; Su, Y.L.; Zhang, Y.Y.; Li, L.; Li, Q.W.; Geng, F.X.; et al. Noble metal-comparable SERS enhancement from semiconducting metal oxides by making oxygen vacancies. *Nat. Commun.* **2015**, *6*, 7800. [[CrossRef](#)]
86. Keshavarz, M.; Tan, B.; Venkatakrisnan, K. Label-free SERS quantum semiconductor probe for molecular-level and in vitro cellular detection: A noble-metal-free methodology. *ACS Appl. Mater. Interfaces* **2018**, *10*, 34886–34904. [[CrossRef](#)] [[PubMed](#)]

87. He, Y.; Su, S.; Xu, T.T.; Zhong, Y.L.; Zapien, J.A.; Li, J.; Fan, C.H.; Lee, S.T. Silicon nanowires-based highly-efficient SERS-active platform for ultrasensitive DNA detection. *Nano Today* **2011**, *6*, 122–130. [[CrossRef](#)]
88. Li, J.F.; Huang, Y.F.; Ding, Y.; Yang, Z.L.; Li, S.B.; Zhou, X.S.; Fan, F.R.; Zhang, W.; Zhou, Z.Y.; Wu, D.Y.; et al. Shell-isolated nanoparticle-enhanced Raman spectroscopy. *Nature* **2010**, *464*, 392–395. [[CrossRef](#)]
89. Joseph, V.; Engelbrekt, C.; Zhang, J.D.; Gernert, U.; Ulstrup, J.; Kneipp, J. Characterizing the kinetics of nanoparticle-catalyzed reactions by surface-enhanced Raman scattering. *Angew. Chem. Int. Ed.* **2012**, *51*, 7592–7596. [[CrossRef](#)]
90. Kang, L.L.; Xu, P.; Zhang, B.; Tsai, H.H.; Han, X.J.; Wang, H.L. Laser wavelength- and power-dependent plasmon-driven chemical reactions monitored using single particle surface enhanced Raman spectroscopy. *Chem. Commun.* **2013**, *49*, 3389–3391. [[CrossRef](#)]
91. Zhang, K.; Zhao, J.J.; Ji, J.; Liu, B.H. Synthesis of micro-sized shell-isolated 3D plasmonic superstructures for in situ single-particle SERS monitoring. *Nanoscale* **2016**, *8*, 7871–7875. [[CrossRef](#)]
92. Zhang, Z.Y.; Kneipp, J. Mapping the inhomogeneity in plasmonic catalysis on supported gold nanoparticles using surface-enhanced Raman scattering microspectroscopy. *Anal. Chem.* **2018**, *90*, 9199–9205. [[CrossRef](#)] [[PubMed](#)]
93. Xie, W.; Schlucker, S. Hot electron-induced reduction of small molecules on photorecycling metal surfaces. *Nat. Commun.* **2015**, *6*, 7570. [[CrossRef](#)] [[PubMed](#)]
94. Zhang, Z.L.; Deckert-Gaudig, T.; Singh, P.; Deckert, V. Single molecule level plasmonic catalysis—a dilution study of p-nitrothiophenol on gold dimers. *Chem. Commun.* **2015**, *51*, 3069–3072. [[CrossRef](#)] [[PubMed](#)]
95. Zhang, K.; Liu, Y.J.; Wang, Y.N.; Zhao, J.J.; Liu, B.H. Direct SERS tracking of a chemical reaction at a single 13 nm gold nanoparticle. *Chem. Sci.* **2019**, *10*, 1741–1745. [[CrossRef](#)]
96. De Nijs, B.; Benz, F.; Barrow, S.J.; Sigle, D.O.; Chikkaraddy, R.; Palma, A.; Carnegie, C.; Kamp, M.; Sundararaman, R.; Narang, P.; et al. Plasmonic tunnel junctions for single-molecule redox chemistry. *Nat. Commun.* **2017**, *8*, 994. [[CrossRef](#)]
97. Tian, Z.Q.; Ren, B.; Li, J.F.; Yang, Z.L. Expanding generality of surface-enhanced Raman spectroscopy with borrowing SERS activity strategy. *Chem. Commun.* **2007**, *34*, 3514–3534. [[CrossRef](#)]
98. Joachim, C.; Gimzewski, J.K.; Aviram, A. Electronics using hybrid-molecular and mono-molecular devices. *Nature* **2000**, *408*, 541–548. [[CrossRef](#)]
99. Kiguchi, M.; Tal, O.; Wohlthat, S.; Pauly, F.; Krieger, M.; Djukic, D.; Cuevas, J.C.; van Ruitenbeek, J.M. Highly conductive molecular junctions based on direct binding of benzene to platinum electrodes. *Phys. Rev. Lett.* **2008**, *101*, 046801. [[CrossRef](#)]
100. Kaneko, S.; Murai, D.; Marques-Gonzalez, S.; Nakamura, H.; Komoto, Y.; Fujii, S.; Nishino, T.; Ikeda, K.; Tsukagoshi, K.; Kiguchi, M. Site-selection in single-molecule junction for highly reproducible molecular electronics. *J. Am. Chem. Soc.* **2016**, *138*, 1294–1300. [[CrossRef](#)]
101. Han, R.; Song, W.; Wang, X.; Mao, Z.; Han, X.X.; Zhao, B. Investigation of charge transfer at the TiO₂-MBA-Au interface based on surface-enhanced Raman scattering: SPR contribution. *Phys. Chem. Chem. Phys.* **2018**, *20*, 5666–5673. [[CrossRef](#)]
102. Li, Y.; Doak, P.; Kronik, L.; Neaton, J.B.; Natelson, D. Voltage tuning of vibrational mode energies in single-molecule junctions. *Proc. Natl. Acad. Sci. USA* **2014**, *111*, 1282–1287. [[CrossRef](#)] [[PubMed](#)]
103. Li, W.; Zhou, J.; Maccaferri, N.; Krahne, R.; Wang, K.; Garoli, D. Enhanced optical spectroscopy for multiplexed DNA and protein-sequencing with plasmonic nanopores: Challenges and prospects. *Anal. Chem.* **2022**, *94*, 503–514. [[CrossRef](#)] [[PubMed](#)]
104. Qi, J.; Zeng, J.B.; Zhao, F.S.; Lin, S.H.; Raja, B.; Strych, U.; Willson, R.C.; Shih, W.C. Label-free, in situ SERS monitoring of individual DNA hybridization in microfluidics. *Nanoscale* **2014**, *6*, 8521–8526. [[CrossRef](#)] [[PubMed](#)]
105. Zhou, J.; Zhou, P.L.; Shen, Q.; Ahmed, S.A.; Pan, X.T.; Liu, H.L.; Ding, X.L.; Li, J.; Wang, K.; Xia, X.H. Probing multidimensional structural information of single molecules transporting through a sub-10 nm conical plasmonic nanopore by SERS. *Anal. Chem.* **2021**, *93*, 11679–11685. [[CrossRef](#)]
106. Olschewski, K.; Kammer, E.; Stockel, S.; Bocklitz, T.; Deckert-Gaudig, T.; Zell, R.; Cialla-May, D.; Weber, K.; Deckert, V.; Popp, J. A manual and an automatic TERS based virus discrimination. *Nanoscale* **2015**, *7*, 4545–4552. [[CrossRef](#)]
107. He, Z.; Han, Z.H.; Kizer, M.; Linhardt, R.J.; Wang, X.; Sinyukov, A.M.; Wang, J.Z.; Deckert, V.; Sokolov, A.V.; Hu, J.; et al. Tip-enhanced Raman imaging of single-stranded DNA with single base resolution. *J. Am. Chem. Soc.* **2019**, *141*, 753–757. [[CrossRef](#)]
108. He, Z.; Qiu, W.W.; Kizer, M.E.; Wang, J.Z.; Chen, W.C.; Sokolov, A.V.; Wang, X.; Hu, J.; Scully, M.O. Resolving the sequence of RNA strands by tip-enhanced Raman spectroscopy. *ACS Photonics* **2021**, *8*, 424–430. [[CrossRef](#)]
109. Hubarevich, A.; Huang, J.A.; Giovannini, G.; Schirato, A.; Zhao, Y.Q.; Maccaferri, N.; De Angelis, F.; Alabastri, A.; Garoli, D. lambda-DNA through porous materials-surface-enhanced Raman scattering in a simple plasmonic nanopore. *J. Phys. Chem. C* **2020**, *124*, 22663–22670. [[CrossRef](#)]
110. Belkin, M.; Chao, S.H.; Jonsson, M.P.; Dekker, C.; Aksimentiev, A. Plasmonic nanopores for trapping, controlling displacement, and sequencing of DNA. *ACS Nano* **2015**, *9*, 10598–10611. [[CrossRef](#)]
111. Dekker, C. Solid-state nanopores. *Nat. Nanotechnol.* **2007**, *2*, 209–215. [[CrossRef](#)]
112. Cao, J.; Liu, H.L.; Yang, J.M.; Li, Z.Q.; Yang, D.R.; Ji, L.N.; Wang, K.; Xia, X.H. SERS detection of nucleobases in single silver plasmonic nanopores. *ACS Sens.* **2020**, *5*, 2198–2204. [[CrossRef](#)]
113. Yang, J.M.; Jin, L.; Pan, Z.Q.; Zhou, Y.; Liu, H.L.; Ji, L.N.; Xia, X.H.; Wang, K. Surface-enhanced Raman scattering probing the translocation of DNA and Amino acid through plasmonic nanopores. *Anal. Chem.* **2019**, *91*, 6275–6280. [[CrossRef](#)] [[PubMed](#)]
114. Zong, C.; Chen, C.J.; Wang, X.; Hu, P.; Liu, G.K.; Ren, B. Single-molecule level rare events revealed by dynamic surface-enhanced Raman spectroscopy. *Anal. Chem.* **2020**, *92*, 15806–15810. [[CrossRef](#)] [[PubMed](#)]

115. Oyamada, N.; Minamimoto, H.; Murakoshi, K. Room-Temperature Molecular Manipulation via Plasmonic Trapping at Electrified Interfaces. *J. Am. Chem. Soc.* **2022**, *144*, 2755–2764. [[CrossRef](#)] [[PubMed](#)]
116. Long, L.; Chen, J.F.; Yu, H.K.; Li, Z.Y. Strong optics force of a molecule enabled by the plasmonic nanogap hot spot in a tip-enhanced Raman spectroscopy system. *Photonics Res.* **2020**, *8*, 1573–1579. [[CrossRef](#)]
117. Keller, E.L.; Brandt, N.C.; Cassabaum, A.A.; Frontiera, R.R. Ultrafast surface-enhanced Raman spectroscopy. *Analyst* **2015**, *140*, 4922–4931. [[CrossRef](#)]